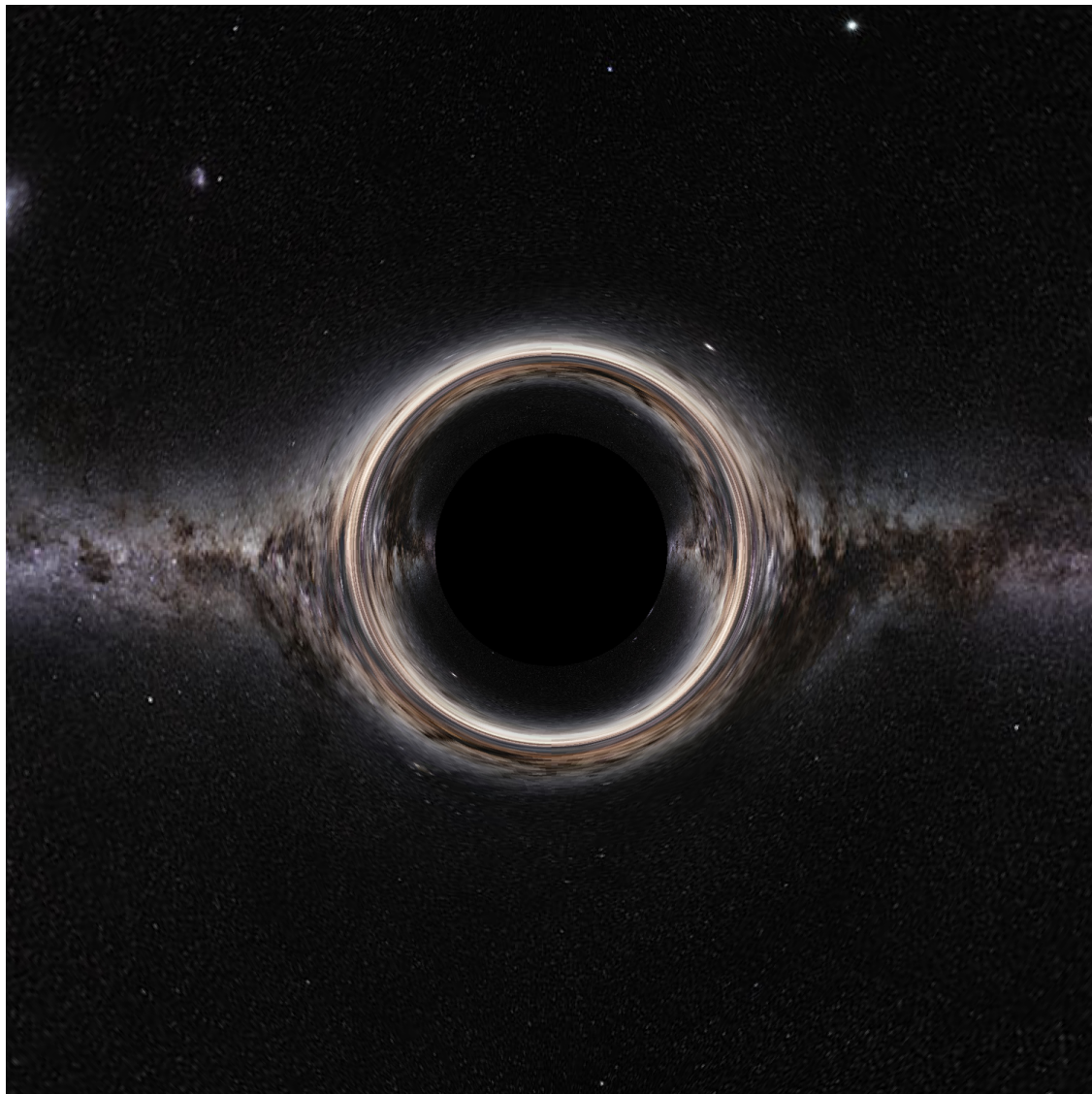


# Schwarzschild Ray Tracing Project Report

Ryan Chen, Sunny Cho, Luca Nacamu, Ziqiu Zhao, Joey Tremonti  
PHYS 129L  
Professor David Berenstein

June 9 2025



# 1 Introduction

In this project, we simulated how light rays behave when they pass close to a Schwarzschild black hole. By numerically integrating geodesic equations in the equatorial plane, we recreated the light-bending effects and visualized the resulting image that an observer would see. The goal is to build the computationally rigorous photo of how light travels by following the Schwarzschild metric tensor.

## 1.1 The Schwarzschild Black Hole

Black holes are the most extreme predictions of general relativity. A Schwarzschild black hole is a non-rotating and non-charged black hole. The gravitational field created by this black hole is so large that at  $R = 2M$ , the light cannot even escape. Large gravitational bends in space-time and light trajectory bending effects lead to observable phenomena such as gravitational lensing. Understanding these effects is essential for interpreting observations from our telescopes and for testing predictions of general relativity. We use the Schwarzschild metric tensor to tell us about the light path.

## 1.2 Ray Tracing

Ray tracing is a technique used to simulate the perception of objects by a camera. In principle, light is emitted in all directions. For the light ray that reflects to our eye, we perceive that as an object. However, this forward-tracing approach is highly inefficient, as it requires evaluating an infinite number of possible photon paths, most of which do not contribute to the final image. To address this, inverse ray tracing is used. Instead of tracing rays from the object, they are traced from the observer into the object. By determining which ray interacts with the objects, we can reconstruct the visual received by the observer. This approach is better than forward ray tracing since it is only considering the relevant light path. In the context of black holes, ray tracing becomes more complex. It is an extreme case where there is an intense gravitational field, so we cannot regard the light as moving in a straight line. Instead, we have to follow the curved geodesic to follow the light path. By integrating ODE generated from the Schwarzschild metrics and energy conservation, we can trace each light ray. This allows us to visualize what we will see when there is a black hole in the middle of the observer and the object.

# 2 Theory & Methodology

## 2.1 Schwarzschild Geometry and Photon Trajectories

A non-rotating black hole is described by the Schwarzschild metric, which in standard coordinates  $(t, r, \theta, \phi)$  takes the form:

$$ds^2 = - \left(1 - \frac{2M}{r}\right) dt^2 + \left(1 - \frac{2M}{r}\right)^{-1} dr^2 + r^2 d\theta^2 + r^2 \sin^2 \theta d\phi^2,$$

where  $M$  is the mass parameter of the black hole (in geometrized units,  $G = c = 1$ ). Since photons move along null geodesics ( $ds^2 = 0$ ), their paths are determined by this metric. We restrict attention to the equatorial plane ( $\theta = \pi/2$ ), in which case the line element becomes

$$0 = - \left(1 - \frac{2M}{r}\right) t^2 + \left(1 - \frac{2M}{r}\right)^{-1} \dot{r}^2 + r^2 \dot{\phi}^2,$$

where dots denote derivatives with respect to an affine parameter  $\lambda$ .

Two conserved quantities follow from the symmetries of this metric:

1. **Energy conservation:** From stationarity ( $\partial_t$  is a Killing vector),

$$E = \left(1 - \frac{2M}{r}\right) \dot{t},$$

which remains constant along each photon trajectory.

2. **Angular momentum conservation:** From axisymmetry ( $\partial_\phi$  is a Killing vector),

$$L = r^2 \dot{\phi},$$

which is likewise constant.

Using  $ds^2 = 0$ , we obtain the effective radial equation:

$$\dot{r}^2 = E^2 - \left(1 - \frac{2M}{r}\right) \frac{L^2}{r^2}.$$

In numerical form, it is convenient to work with a first-order system of ODEs for the variables  $(t(\lambda), r(\lambda), \phi(\lambda), p_r(\lambda))$ , where  $p_r = \dot{r}$ . The remaining components  $\dot{t}$  and  $\dot{\phi}$  are computed algebraically from  $E$  and  $L$ .

## 2.2 Equations of Motion

We introduce the following state variables along each photon geodesic:

- $t(\lambda)$ : coordinate time,
- $r(\lambda)$ : radial coordinate,
- $\phi(\lambda)$ : angular coordinate in the equatorial plane,
- $p_r(\lambda) \equiv \dot{r}(\lambda)$ : radial momentum.

With the constants  $E$  and  $L$ , the geodesic equations in first-order form become:

$$\dot{t} = \frac{E}{1 - \frac{2M}{r}}, \tag{1}$$

$$\dot{\phi} = \frac{L}{r^2}, \tag{2}$$

$$\dot{r} = p_r, \tag{3}$$

$$\dot{p}_r = -\frac{M}{r^2} \left(1 - \frac{2M}{r}\right)^{-2} E^2 + \frac{L^2}{r^3} \left(1 - \frac{2M}{r}\right) - \frac{ML^2}{r^4}. \tag{4}$$

The expression for  $\dot{p}_r$  follows from combining the radial geodesic equation with the null-condition consistency. At each integration step,  $\dot{t}$  and  $\dot{\phi}$  are updated algebraically using  $E$  and  $L$ .

## 2.3 Simulation Environment Setup

There are a few operational terms that will be referred to:

- Black Hole
  - Mass parameter,  $M$
  - Schwarzschild radius,  $r_s = 2M$
  - Photon-sphere radius,  $r_{\text{ph}} = 3M$
  - Critical impact parameter,  $b_{\text{crit}} = 3\sqrt{3} M$
  - Capture softening factor,  $s$  (e.g.  $s = 1.1$ )
- Observer
  - Radial location,  $r_{\text{obs}}$
  - Cartesian position,  $\vec{r}_{\text{obs}} = (r_{\text{obs}}, 0, 0)$
  - Local orthonormal triad,  $\{\hat{r}, \hat{\theta}, \hat{\phi}\}$
- Image-plane offset,  $\epsilon$
- Camera & Image Plane
  - Field of view (full), FOV
  - Half-angle,  $\alpha = \frac{\text{FOV}}{2}$
  - Image-plane width,  $L = 2\epsilon \tan \alpha$
  - Pixel resolution,  $P \times P$
  - Pixel indices,  $(i, j) \in \{0, \dots, P-1\}^2$
  - Heading vector,  $\hat{h}_{ij}$
- Photon / Ray Variables
  - Conserved energy,  $E$

- Conserved angular momentum,  $L$
- Impact parameter,  $b = r_{\text{obs}} \sin \alpha$
- Four-momentum,  $p^\mu = (p^t, p^r, p^\theta, p^\phi)$
- Affine parameter,  $\lambda$
- Equatorial-rotation angle,  $\beta$
- Integration Parameters
  - Step size,  $\Delta\lambda$
  - Number of steps,  $N_\lambda$
  - Symplectic order,  $n$  (e.g.  $n = 2$ )
  - Coupling parameter,  $\omega$
  - Outer boundary radius,  $r_{\text{bounds}}$
- Ray Classification
  - **BH** (captured)
  - **BG** (mapped background)
  - **IN** (still in bounds after  $N_\lambda$ )
  - Apparent shadow radius,  $R_{\text{shadow}} \simeq 2.6 r_s$
- Background Patch
  - Centre angles,  $(\theta_*, \phi_*)$
  - Angular extents,  $(\Delta\theta, \Delta\phi)$
  - Texture coordinates,  $(u, v)$  (equirectangular map)

We imagine an observer located far from the **black hole** at  $r_{\text{obs}} \gg 2M = r_s$ . The flat coordinates are represented with the standard Cartesian  $(x, y, z)$ . The **observer** sits on the  $x$ -axis at some  $x = r_{\text{obs}}$ :  $\vec{r}_{\text{obs}} = (r_{\text{obs}}, 0, 0)$ .

We wish to *send rays in the general direction of the black hole* at some **FOV** (Field of View). FOV describes the angle of the entire cone, so the half-angle is the deviation from the optical axis.

We send rays at angular deviations  $\alpha_\perp \in [0, \text{FOV}/2]$  in the **optical axis** direction  $-\hat{r} = -\hat{x}$ . As the FOV is for width, the diagonal has larger  $\alpha$  bounds:  $\alpha_{\text{diag}} \in [0, \arccos(\cos(\text{FOV}/2))]$

The **image plane** is a square on a plane perpendicular to the line that connects the observer and the black hole (origin). The center of the image plane must be close to the observer, so that the space-time distortion is minimal between the image and the observer.

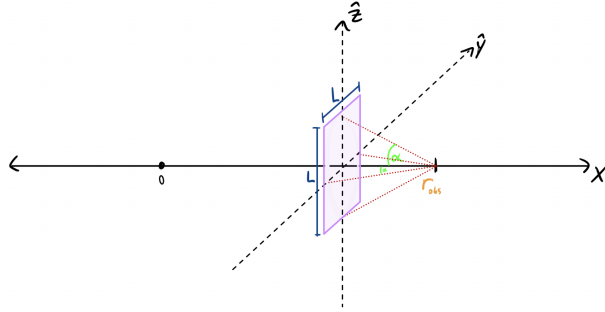


Figure 1: Image Plane Diagram

Let a small  $\epsilon$  be the distance from the center of the image plane to the observer. So the square width can be determined:  $L = 2\epsilon \tan(\alpha_{\perp_{\max}}) = 2\epsilon \tan(\text{FOV}/2)$

The image plane bounds can be described as:

$$A_{\text{im}} = (r_{\text{obs}} - \epsilon, [-L/2, L/2], [-L/2, L/2])$$

## 2.4 Image Plane Pixel Mapping and Initial Conditions

We begin with a chosen FOV, and Image Resolution (denote as  $P$ ). Naturally, we have an image with  $P^2$  pixels. We traverse through them as such:  $i, j \in \{0, 1, 2, \dots, P - 1\}$ , in standard (row,col) format.

The center of the image is located at

$$\vec{A}_0 = (r_{\text{obs}} - \epsilon, 0, 0)$$

The center of each pixel is located at:

$$\vec{A}_{ij} = \vec{A}_0 + \begin{pmatrix} \text{Pixel Proportion (half offset)} \\ \frac{i+0.5}{P} \\ -0.5 \\ \text{Centering} \end{pmatrix} P_{\text{right}} \hat{y} + \left( \frac{j+0.5}{P} - 0.5 \right) P_{\text{ratio}}^{\text{scale}} \hat{z}$$

With the pixel centers  $\vec{A}_{ij}$  in hand we define the *flat-space heading vector* (this is why  $\epsilon$  must be small, we're making an approximation)

Close-up 3D Scene: Observer, Image Plane, Event Horizon

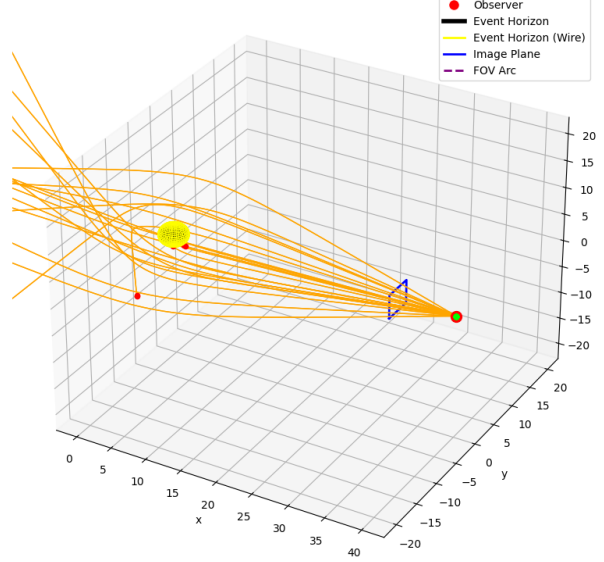


Figure 2: Randomly Sampled Rays Emitted at a 30 Degree Arc Through Image Plane

$$\vec{h}_{ij} = \vec{A}_{ij} - \vec{r}_{\text{obs}} \in \mathbb{R}^3, \quad (5)$$

and its unit version  $\hat{h}_{ij} = \vec{h}_{ij}/\|\vec{h}_{ij}\|$ . Two further steps are needed before the geodesic integrator can be invoked.

#### 2.4.1 Rotating the Initial Trajectory to the Equatorial Plane

The metric coefficient  $g^{\phi\phi} = 1/(r^2 \sin^2 \theta)$  diverges for<sup>1</sup>  $\theta \rightarrow 0, \pi$ . In practice this shows up as a vertical “seam” at  $\phi = \pi$  in the background texture; photons whose initial direction is even *slightly* off-equatorial accumulate large numerical errors once their trajectories stray near the poles.

Schwarzschild space-time is spherically symmetric, so angular momentum is conserved and the geodesic path is a planar embedding. We exploit this by *rotating* every initial ray so that its plane of motion coincides with the equator ( $\theta = \pi/2$ ), integrate the geodesic there—where  $\sin \theta = 1$  and  $g^{\phi\phi}$  is perfectly regular—and finally rotate the hit-point back to the laboratory frame.

For a normalized heading  $\hat{h}$  the signed angle between its projection onto the  $yz$ -plane and the  $y$ -axis is<sup>2</sup>

$$\beta = \text{arctan}_2(h_z, h_y),$$

<sup>1</sup>At  $\theta = 0$  or  $\theta = \pi$  the coordinate  $\phi$  is undefined; a tiny floating-point error in either the integrator or the texture-mapping routine therefore blows up as  $1/\sin \theta$ .

<sup>2</sup>The `arctan2` function belongs to the `numpy` library, and is special in that it preserves the angle’s relation to an axis, making it usable universally for rays emitted at any ( $yz$ ) quadrant.

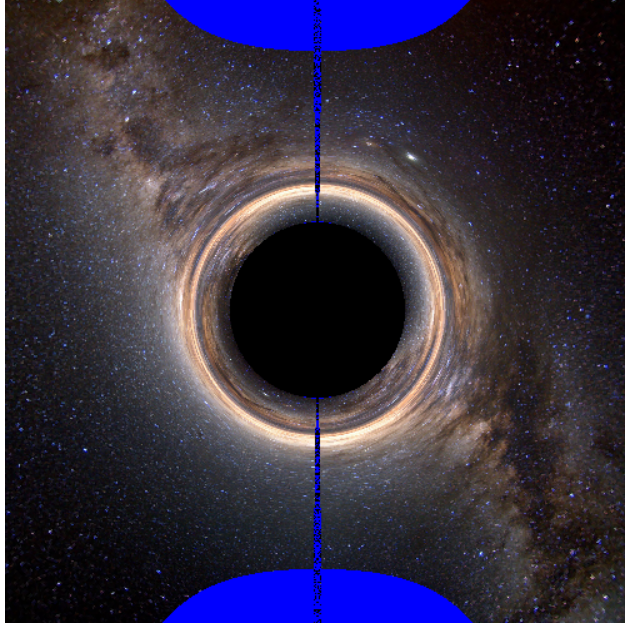


Figure 3:  $\phi = \pi$  vertical seam. Blue pixels are for diagnostic purposes, indicating that the ray hit the simulation boundary but not the Schwarzschild nor the background image.

positive for upward-pointing rays ( $h_z > 0$ ). A clockwise rotation by  $-\beta$  about  $\hat{x}$  brings the vector into the equatorial plane:

$$\hat{h}' = R_x(-\beta)\hat{h}, \quad R_x(\gamma) = \begin{pmatrix} 1 & 0 & 0 \\ 0 & \cos \gamma & -\sin \gamma \\ 0 & \sin \gamma & \cos \gamma \end{pmatrix}.$$

When the simulation is finished, we can simply apply the inverse rotation  $R_x(+\beta_{ij})$  associated to every ray.

With this “tilt–integrate–untilt” strategy the vertical seam disappears (Fig. 7), and the numerical accuracy of the Euler-step integrator is now limited by the chosen affine step size  $\Delta\lambda$  rather than by the coordinate pathology at  $\theta = 0, \pi$ .

#### 2.4.2 From Cartesian Direction to Spherical Basis Components

At the observer’s location we place the local orthonormal triad

$$\{\hat{r}, \hat{\theta}, \hat{\phi}\} = \{+\hat{x}, -\hat{z}, +\hat{y}\},$$

valid because the observer sits on the  $+x$ -axis and the equatorial plane ( $\theta = \pi/2$ ). Projecting the unit heading vector  $\hat{h}_{ij}$  onto this triad gives the *orthonormal-frame* components

$$p_{ij}^{\hat{r}} = -\hat{h}_{ij} \cdot \hat{x}, \quad p_{ij}^{\hat{\theta}} = -\hat{h}_{ij} \cdot \hat{z}, \quad p_{ij}^{\hat{\phi}} = \hat{h}_{ij} \cdot \hat{y},$$

with  $\|\mathbf{p}^i\| = 1$  by construction.

**Coordinate–basis components.** EinsteinPy expects momenta in the *coordinate* basis  $\{\partial_r, \partial_\theta, \partial_\phi\}$ . For an equatorial, static observer in Schwarzschild spacetime the orthonormal vectors are related to the coordinate basis by

$$\hat{e}_{\hat{r}} = \sqrt{1 - \frac{2M}{r_{\text{obs}}}} \partial_r, \quad \hat{e}_{\hat{\theta}} = \frac{1}{r_{\text{obs}}} \partial_\theta, \quad \hat{e}_{\hat{\phi}} = \frac{1}{r_{\text{obs}}} \partial_\phi.$$

Hence

$$\boxed{\begin{aligned} p^r &= \frac{p^{\hat{r}}}{\sqrt{1 - 2M/r_{\text{obs}}}}, \\ p^\theta &= \frac{p^{\hat{\theta}}}{r_{\text{obs}}}, \\ p^\phi &= \frac{p^{\hat{\phi}}}{r_{\text{obs}}}. \end{aligned}}$$

Because the observer lies in the equatorial plane ( $\theta = \pi/2$ ), the usual  $\sin \theta$  factor in  $p^\phi$  reduces to unity.

**Normalisation choice.** Null geodesics are invariant under the rescaling  $p^\mu \mapsto k p^\mu$  ( $k > 0$ ); only their *direction* fixes the orbit, while  $k$  fixes the affine parameter  $\lambda$ . We adopt the convention

$$\|\hat{\mathbf{p}}^i\| = 1$$

so that a single integrator step  $\Delta q^\mu = p^\mu \Delta \lambda$  corresponds to a *unit* spatial displacement in the local frame. With EinsteinPy's fixed-step integrator this keeps the local truncation error essentially uniform across the field of view: enlarging  $\|\hat{\mathbf{p}}^i\|$  by a factor  $k$  would enlarge every physical step by the same  $k$  and accumulate error linearly with distance from the optical axis.

In summary, the conversion implemented in `angles_to_p_sph` is

$$(p^r, p^\theta, p^\phi) = \left( -\frac{\cos a \cos b}{\sqrt{1 - 2M/r_{\text{obs}}}}, -\frac{\sin b}{r_{\text{obs}}}, \frac{\sin a \cos b}{r_{\text{obs}}} \right),$$

where  $a$  and  $b$  are the right and up angle deflections. after which `build_null_4momentum_ep_sph` solves the null condition for  $p^t$ . We can now calculate the trajectory associated with every pixel:  $\mathbf{p}_{0_{ij}}$ .

All rays are emitted from the observer, so  $\mathbf{q}_0$  is the same for all  $i, j$ . Let the time component  $\mathbf{q}_0^t = 0$ .

With this, our initial conditions  $\mathbf{q}_0, \mathbf{p}_{0_{ij}}$  are created.

## 2.5 Numerical Integration with EinsteinPy

We propagate every null ray with the FANTASY integrator shipped with the EINSTEINPY<sup>3</sup> package. Unlike the library's default Runge–Kutta routine FANTASY uses a *fixed-step, symplectic* scheme which preserves the Hamiltonian flow splitting and therefore keeps long-term energy errors bounded.

This integrator was adapted to run on GPUs via Numba's Nvidia CUDA API support to exploit massive parallelization and vectorization benefits.

1. **Metric.** We instantiate the contravariant Schwarzschild metric  $g^{\mu\nu}(r, \theta)$  with mass parameter  $M$  via `einsteinpy.metric.Schwarzschild`. All quantities are in geometrised units ( $G = c = 1$ ).
2. **Initial data.** For each pixel the four-position and *spatial* momentum in Schwarzschild coordinates have already been determined:

$$\mathbf{q}_0 \quad \mathbf{p}_0$$

3. **Integrator setup.** Example Arguments:

- integration order: 2
- step size (affine):  $\Delta\lambda = 0.01$
- number of steps:  $N_\lambda = 2 \times 10^5$
- coupling parameter:  $\omega = 0.001$  (lower is better for capture/grazing trajectories)

---

<sup>3</sup>P. Christian & C.-K. Chan, “FANTASY: user-friendly symplectic geodesic integrator for arbitrary metrics with automatic differentiation”, *Astrophys. J.* **909**, 67 (2021).

Hence the affine range is  $\lambda \in [0, N_\lambda \Delta \lambda]$ . During stepping we terminate early once  $r \leq r_s \cdot s$  (*capture*) or  $r \geq r_{\text{bounds}}$  (*escape*). We chose  $s = 1.1$  as a softening parameter for early capture since there is massive numerical instability approaching  $r_s$ .

Once all the affine steps were ran through, or the simulation exited early, the final  $\mathbf{q}, \mathbf{p}$  are returned.

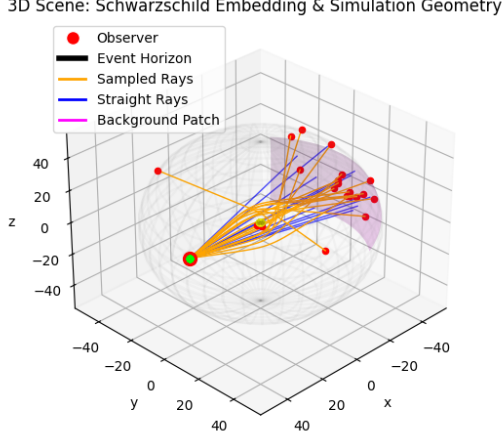


Figure 4: Sampled Rays Trajectories Emitted at a 30 Degree Arc

## 2.6 Ray-to-Image Classification

For every detector pixel  $(i, j) \in \{0, \dots, P - 1\}^2$  we fire a null geodesic with initial heading  $\hat{h}_{ij}$  (Sec. 2.4). After numerical integration each ray ends up in one of three *mutually-exclusive* groups:

**BH (captured)** The ray plunges when either (a) its path crosses the horizon  $r \leq r_s \cdot s$  or (b) its initial impact parameter  $b = r_{\text{obs}} \sin \alpha$  is below the critical value of the photon ring ( $r = 3M$ ):

$$b_{\text{crit}} = 3\sqrt{3} M, \quad \alpha_{\text{crit}} = \arcsin\left(\frac{b_{\text{crit}}}{r_{\text{obs}}}\right).$$

Pixels in this set are painted **black**, forming a shadow with apparent radius  $R_{\text{shadow}} \simeq 2.6 r_s$ —much larger than the horizon itself.

**BG (mapped background)** If the trajectory exits the domain at the simulation boundary sphere  $r = r_{\text{bounds}}$  we treat the last direction  $(\theta_\infty, \phi_\infty)$  as the ray's arrival point. Given a well-selected  $r = r_{\text{bounds}}$ —that is any  $r > 10M$ —curvature is minimal and the trajectory is approximately straight, so its relative angle is constant.

A user-selected *background patch* is defined by the angular bounds

$$\theta_* \pm \frac{\Delta\theta}{2}, \quad \phi_* \pm \frac{\Delta\phi}{2}.$$

The ray contributes to the image *iff*  $|\theta_\infty - \theta_*| \leq \Delta\theta/2$  and  $|\phi_\infty - \phi_*|_{\text{mod } 2\pi} \leq \Delta\phi/2$ . Its texture coordinates are then

$$u = \frac{\theta_\infty - \theta_* + \Delta\theta/2}{\Delta\theta}, \quad v = \frac{\phi_\infty - \phi_* + \Delta\phi/2}{\Delta\phi},$$

and the RGB value sampled from the **background image**<sup>4</sup> is copied to pixel  $(i, j)$ . This is known as **equirectangular mapping**. Rays escaping *outside* the patch (diagnostics) are coloured **blue**.

<sup>4</sup>With an equirectangular panorama, the patch covers the entire sphere:  $(\Delta\theta = \pi, \Delta\phi = 2\pi)$ , but the angular bounds of the image can be arbitrarily chosen

**IN (still integrating)** Extremely grazing rays that reach the step limit without meeting either criterion above are rare; in debug renders they are marked **red** but are ignored in production images.

Iterating over the full  $P \times P$  grid yields the final colour buffer combining the black-hole shadow with the gravitationally-lensed background.

### 2.6.1 On Equirectangular Projection and Field-of-View

The sky panorama is stored in an *equirectangular* map<sup>5</sup>

$$(\theta, \phi) \mapsto (u, v) = \left( \frac{\theta}{\pi}, \frac{\phi + \pi}{2\pi} \right),$$

so equal steps in  $(u, v)$  correspond to equal angular steps on the celestial sphere.

A square camera field-of-view of width  $\text{FOV} = \Delta\theta = \Delta\phi$  is centered on  $(\theta_*, \phi_*)$ :

$$\theta \in [\theta_* - \frac{\text{FOV}}{2}, \theta_* + \frac{\text{FOV}}{2}], \quad \phi \in [\phi_* - \frac{\text{FOV}}{2}, \phi_* + \frac{\text{FOV}}{2}].$$

This rectangle is sampled on a uniform  $P \times P$  lattice; As the  $(u, v)$  texture coordinates are a ratio, we simply multiply it by the pixel dimensions of the background patch image (and round it) to find the pixel index of the image.

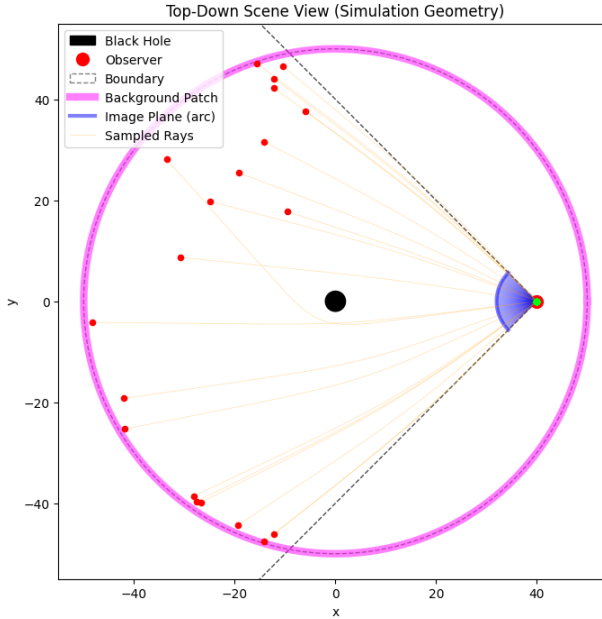


Figure 5: X-Y Cross-Section of Scene, Background Image Projected on Entire Sphere

---

<sup>5</sup> $(\theta, \phi)$  are standard spherical coordinates measured from the  $+z$  axis and  $+x$  axis, respectively.

## 2.7 Summary of Workflow

### 1. Initialize physical & numerical parameters

- *Black-hole scale.* Mass  $M=1$  ( $\Rightarrow r_s = 2M$ ,  $r_{\text{ph}} = 3M$ ).
- *Observer.* Radius  $r_{\text{obs}} = 10M$ ; Cartesian position  $\vec{r}_{\text{obs}} = (r_{\text{obs}}, 0, 0)$ .
- *Camera.* Square field of view FOV (half-angle  $\alpha = \frac{\text{FOV}}{2}$ ); image plane offset  $\epsilon$ ; resolution  $P \times P$  (e.g.  $400^2$ ).
- *Integrator.* Step size  $\Delta\lambda$ , steps  $N_\lambda$ , symplectic order  $n$  (e.g.  $n = 2$ ), coupling  $\omega$ , outer boundary  $r_{\text{bounds}}$ , capture factor  $c$ .

### 2. Pre-compute constant factors

- Critical impact parameter  $b_{\text{crit}} = 3\sqrt{3} M$ , critical angle  $\alpha_{\text{crit}} = \arcsin(b_{\text{crit}}/r_{\text{obs}})$ .
- Orthonormal triad  $\{\hat{r}, \hat{\theta}, \hat{\phi}\}$  at  $\vec{r}_{\text{obs}}$  and the conversion  $(p^{\hat{r}}) \rightarrow (p^\mu)$ .

### 3. Pixel loop $(i, j) \in \{0, \dots, P - 1\}^2$

- Map pixel centre to angular deflections  $(a_{ij}, b_{ij}) \leftrightarrow (\Theta_{ij}, \Phi_{ij})$ .
- Build unit heading  $\hat{h}_{ij}$ , rotate to equatorial plane  $(\beta_{ij})$ , and convert to initial four-momentum

$$E = 1, \quad L = r_{\text{obs}} \sin \Theta_{ij}, \quad p_0^\mu = (p^t, p^r, p^\theta, p^\phi).$$

- Integrate the null geodesic with FANTASY until  $r \leq c r_s$  (**BH**),  $r \geq r_{\text{bounds}}$  (**BG**), or  $N_\lambda$  steps (**IN**).
- Record escape angles  $(\theta_\infty, \phi_\infty)$  if **BG**.

### 4. Shade pixel

- **BH:** set RGB = black.
- **BG:** convert  $(\theta_\infty, \phi_\infty)$  to texture coords  $(u, v)$  and sample the equirectangular panorama.
- **IN:** optional diagnostic colour (red).

### 5. Assemble and display image

- Collect RGB values into a  $P \times P$  buffer.
- Render the observer's view showing the shadow ( $R_{\text{shadow}} \simeq 2.6 r_s$ ) and the lensed background.

This combination of analytic reduction to first-order geodesic ODEs and robust numerical integration captures the essential physics of light bending in Schwarzschild geometry and produces a simulated image that reflects the characteristic shadow and lensing ring around a black hole.

### 3 Results & Discussion



Figure 6: Original Image of Milky Way Equirectangular Panorama used from ESO [3].

This first image was mapped such that  $\Delta\phi = 2\pi, \Delta\theta = \pi$ , covering the entire sphere.

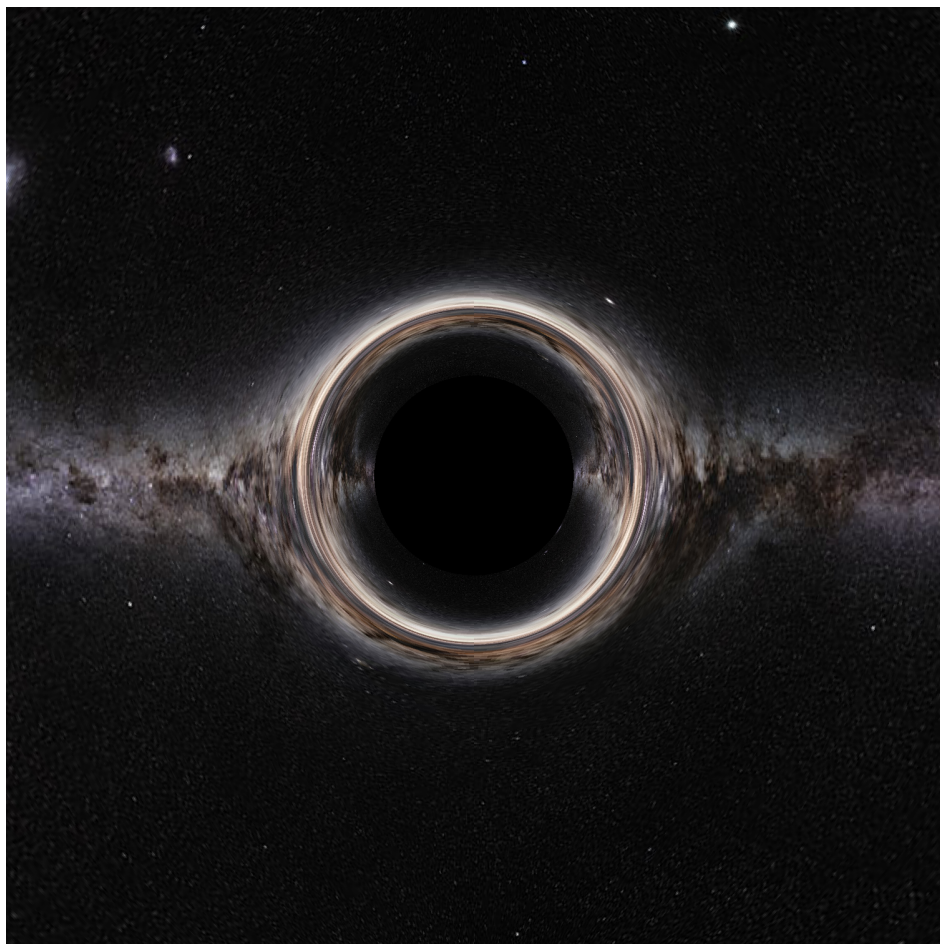


Figure 7: 90 Degree View with Gravitational Lensing

### 3.1 Ray Behavior

In flat spacetime (absence of curvature), light rays travel along straight paths. However, near a Schwarzschild black hole, the intense spacetime curvature dramatically alters photon trajectories. As illustrated in Figure 8, light rays become significantly bent, with those passing close to the photon sphere ( $r = 3M$ ) experiencing extreme deflection.

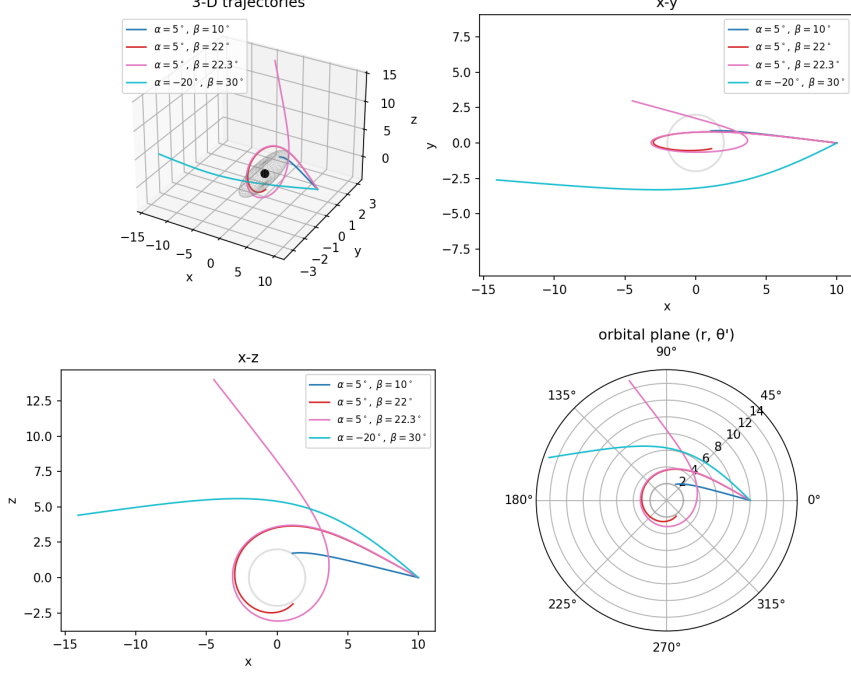


Figure 8: Trajectories of Multiple Rays

### 3.2 Image Formation

The gravitational lensing effects produce several distinctive features in the simulated images:

- **Multiple Imaging:** As shown in Figure 2, light bending causes single objects to appear multiple times around the black hole. This occurs when photons from the same source reach the observer along different paths.
- **Einstein Rings:** Perfect alignment between source, lens, and observer creates complete circular images known as Einstein rings.
- **Behind-the-Hole Vision:** The extreme warping of spacetime allows observation of objects that would normally be obscured behind the black hole, as photons are bent around the event horizon.

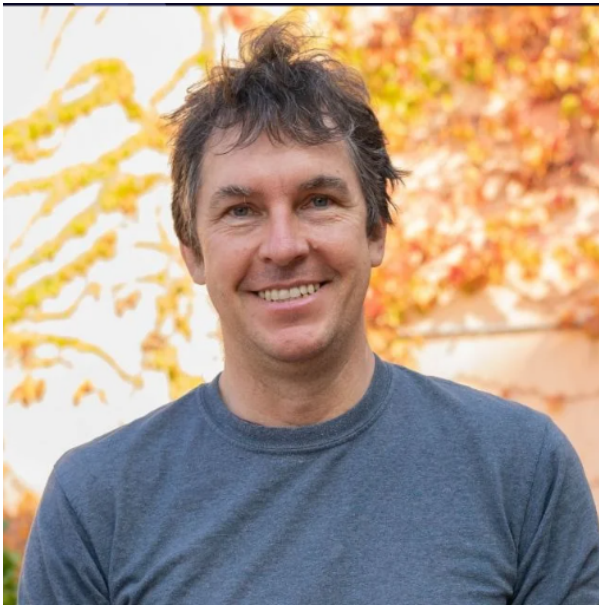


Figure 9: Original image of Prof. Berenstein

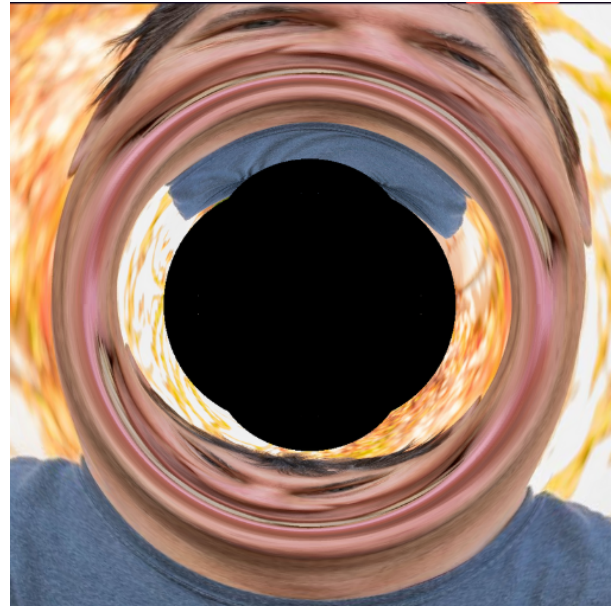


Figure 10: Gravitationally lensed view showing multiple images. Notice the grey shirt appearing twice.

Figure 11: Comparison showing gravitational lensing effects on a human face

### 3.3 Numerical Challenges

Our simulations encountered several technical challenges:

- **Coordinate Singularities:** Near the event horizon ( $r \rightarrow 2M$ ), the Schwarzschild coordinates become singular, leading to numerical instabilities. Similar issue manifests in the  $\phi = \pi$  region where  $1/\sin \phi$  terms diverge, creating visible artifacts as shown in Figure 3.
- **Photon Capture:** Determining the precise boundary between captured and escaping photons requires careful tuning of termination conditions to avoid both premature termination and excessive computation.
- **Precision Issues:** Grazing rays that orbit near the photon sphere require extremely small step sizes to maintain accuracy without becoming computationally prohibitive.

To mitigate these issues, we implemented several solutions:

- Having the event horizon in program slightly larger than  $r = 2M$  so the light rays never reach this coordinate singularity
- Special handling of polar-angle calculations
- Decreasing affine step size  $\Delta\lambda$  and coupling  $\omega$

The final simulations successfully demonstrate all key features of black hole imaging predicted by general relativity while maintaining numerical stability throughout the image plane.

## 4 Conclusion

In this study, we demonstrated how curved spacetime alters the path of light. In the multiple images that we produced by ray tracing, we can see some key features such as dark central disk where the photons are captured inside  $r \leq r_s$ , and bright narrow rings where the photons graze the unstable orbit  $r \approx 3M$ . Not only that, there are arc-shaped distortions and repeats where there is strong lensing of the background, and lastly smooth circular symmetry where it shows the correct handling of the coordinate singularities. This outcome seems to qualitatively match the published simulation and pictures. In Zhu, HanHuan [2] the authors compute the shadow of a Schwarzschild black hole with supertranslation ‘hair’ and find that despite distortions in the photon sphere and a coordinate-dependent shift in the projection, the size and shape of the shadow itself remain identical to the classical Schwarzschild case. Likewise, our Schwarzschild ray tracing likewise produces a circular shadow radius/approximately 2.6 with the expected photon-ring structure. Not only that, based on the Luminent computer simulation of the appearance of a Schwarzschild black hole, his shadow radius and ring morphology match ours almost exactly (without the accretion disk) [1].

However, there are some limitations in our simulation. We assumed that the black hole with the Schwarzschild black hole has zero spin. Besides the real astrophysical holes rotate, which twists spacetime and deforms the shadow. Therefore, it will be a good next step if we use Kerr geometry which implements full ray tracing in the Kerr metric to capture spin induced shadow asymmetry and multiple lensed rings of different width. Not only that, we rotate every ray into the equatorial plane for integration. That enforces planar symmetry; however, that might sample-off equator structure if the observer were tilted. Lastly, we could have resolved sub-photon ring structure or very high order lensed images by using a higher image resolution  $P$ .

In summary, our Schwarzschild ray tracer reproduced all of the signatures of strong field lensing - the oversized dark capture disk and the razor-thin photon ring at  $r \approx 3M$ . The agreement was shown with both analytical theory and classic simulations. Moving forward, extending this pipeline to Kerr spacetime, adopting dull integrators, and boosting to multi-GPU will bring views of black holes closer than ever to what telescopes like the EHT observe.

## References

- [1] Jean-Pierre Luminet, *Image of a Spherical Black Hole with Thin Accretion Disk*, *Astronomy & Astrophysics* **75** (1979), 228–235.
- [2] Qing-Hua Zhu, Yu-Xuan Han, and Qing-Guo Huang, *The Shadow of Supertranslated Schwarzschild Black Hole*, *Eur. Phys. J. C* **83** (2023) 88, arXiv:2205.14554.
- [3] European Southern Observatory, *The Milky Way panorama*, photographic image, credit: ESO/S. Brunier (2009), <https://www.eso.org/public/images/eso0932a/>.